JMEPEG (2015) 24:3643–3650
DOI: 10.1007/s11665-015-1639-2

1059-9495/$19.00

Effect of Machining Configurations on the Electrochemical Response of Mild Steel in 3.5% NaCl Solution

M. Prakash, A.P. Moon, K. Mondal, and S. Shekhar

(Submitted April 6, 2015; in revised form June 22, 2015; published online August 5, 2015)

The present work is based on the study of the electrochemical response of mild steel as a function of machining configurations. The variable parameters were rake angle and turning speed, while feed rate and depth of cut remained fixed. Dynamic polarization tests and electrochemical impedance spectroscopy in 3.5% NaCl solution were done to analyze the electrochemical behavior of mild steels with the variation of rake angle and turning speed. The electrochemical response showed that the steel machined at higher speed and positive rake angle had higher resistance to charge transfer. Similarly, steel machined at lower speed and negative rake angle showed lower resistance to charge transfer. The results obtained in this study suggest that machining on mild steel should be carried out at positive rake angle and at higher speed to have smoother surface finish, strain-relieved surface grains, and subsequently better corrosion resistance, which was measured from corrosion current as determined by the Tafel extrapolation from the polarization plots.

Keywords corrosion, EIS, machining, mild steel, polarization

1. Introduction

Mild steel is one amongst the most common, versatile, and cheap forms of steels, and it is considered as the most reasonable and suitable material for making of wide varieties of heavy machineries and building up of industries related to construction and military applications. In naval applications, like making submarines, ships, docks, etc., different grades of mild steels are used. These applications always experience extreme corrosive environments. On the other hand, components made of steels undergo several manufacturing steps before actual operation. One of the major manufacturing operations is machining.

Machining process is removal mode of processing, where hard machine tool removes metal from the workpiece. Among various machining operations, turning operation is very common and often used in manufacturing. Machining parameters are usually planned for the betterment of surface quality in the form of reducing surface roughness, residual stress, and modification of sub-surface microstructure. These parameters can change independently according to the machining conditions. Selection of appropriate cutting parameters in turning operation is of fundamental importance for generation of good surface finish (Ref 1). The surface quality, obtained after the machining process, has a definite role on the wear resistance, fatigue resistance, corrosion properties, and functional properties of the material (Ref 2-4). Machining process imposes severe plastic deformation (SPD) involving large strain, high strain rates, and high temperature in the deformation zone (Ref 5-7). The chip formed as well as the machined surface experience severe plastic deformation (SPD) during machining, which would cause changes in microstructure. It often generates fine grain size as shown by Shekhar et al. (Ref 8). These effects would finally affect the corrosion and oxidation behavior of the materials.

After machining, which in most of the cases is the final processing operation, the finished part is exposed to, mild to extreme humid or hot conditions, sea water, wastes generated from industry, etc. Surface roughness influences the hydrodynamic and mass-transfer boundary layer, which can further affect the electrochemical and mechano-chemical behavior of a surface. A number of studies have been carried out on the atmospheric corrosion of mild steel (Ref 9-13), but literatures on corrosion behavior of mild steel as a function of machining parameters, like rake angle, speed etc., are very much limited. The study by Ghosh and Kain (Ref 4) has shown that the surface finish affects the stress corrosion behavior of AISI 304L stainless steel. Another report (Ref 14) says that surface finish affects the corrosion behavior of Cu-based alloys. Moreover, a recent analysis on the oxidation behavior of mild steel as a function of machining parameters, like rake angle and cutting speed, shows that surface roughness as well sub-surface microstructure have strong dependency on the oxidation behavior (Ref 15). Thus, the effect of surface roughness is a crucial factor that should be considered in validating the corrosion rate of mild steel from the laboratory experiments. Since machining is unavoidable in many instances of engineering mild steel components, it demands for in-depth studies related to corrosion behavior of mild steel as a function of machining parameters. Recently, we have carried out a series of experiments on a mild steel machined at various rake angle and cutting speed based on salt fog and immersion tests in 3.5% freely aerated NaCl solution. It has been observed that the steel machined at lowest cutting speed and highest rake angle has

M. Prakash, A.P. Moon, K. Mondal, and **S. Shekhar,** Department of Materials Science and Engineering, Indian Institute of Technology Kanpur, Kanpur 208 016, India. Contact e-mail: shashank@iitk.ac.in.

highest corrosion resistance (Ref 16). However, the electrochemical responses (polarization behavior and impedance effect of the machined surface) of the steels machined at various rake angle and cutting speed have not been studied.

Hence in this research, it is intended to bring out the effect of variation of the machining parameters on electrochemical behavior (polarization behavior and impedance effect of the machined surface) of mild steel. The mild steel samples were machined by turning operation at three different rake angles (+20°, 0° and −20°) and three different cutting speeds (41, 276 and 541 m/s), which resulted in nine different sample conditions. In all the cases, depth of cut and feed rate were kept fixed. The polarization behavior was studied using (i) Tafel polarization and (ii) electrochemical impedance spectroscopy (EIS) using 3.5% NaCl solution. The corrosion rate was also measured by Tafel extrapolation. The inter-relation between rake angle and cutting speed with electrochemical polarization behavior (polarization resistance and charge transfer resistance) and corrosion current (as measured from Tafel extrapolation) of the mild steel was established. It is to be mentioned that the sole purpose of the current study is to find the polarization behavior. Corrosion behavior as obtained from the Tafel plots is the corrosion current.

2. Materials and Methods

2.1 Material

The present work was performed on commercially available cylindrical mild steel rod with diameter of 16 mm. The samples were first annealed at 600 °C for 1 h to ensure strain-free equiaxed microstructure. Table 1 shows the composition of the steel sample analyzed by BAIRD SPECTRO VAC DV-6 optical emission spectrometer.

2.2 Machining

A lathe was used for turning operation. Nine sets of mild steel samples (length of machined portion is 25 mm) were prepared. The rake angle and turning speed were changed keeping the depth of cut and feed rate constant. Sharp high-speed steel cutting tool was used for cutting operation.

The samples after machining were designated as 20 L, 20 M, 20 H, 0 L, 0 M, 0 H, −20 L, −20 M, −20 H, and the as-received sample as AS. The numbers indicated the rake angles 0°, 20°, and −20°, and the alphabets, L, M, and H, specified the three different linear cutting speeds: low (L) = 41 mm/s, medium (M) = 276 mm/s, and high (H) = 541 mm/s. The feed rate was 0.177 mm, and depth of cut was 1.5 mm.

2.3 Microstructure

The machined sample was cut horizontal to flat surface to see the cross-sectional microstructure. This was done to see the effect of machining on the surface grain morphology. After cutting, the sample was cleaned ultrasonically in acetone and then mounted on epoxy resin followed by mechanically grinding on 120, 240, 320, 600, 800, 1000, 1200, and 1600 grit silicon carbide abrasive papers progressively. Cloth polishing was done with the use of a colloidal suspension of Al_2O_3 (0.05 μm sized) in water. Special attention was given to the machined edges of the samples. After preparation of surface, etching was done using 2% Nital solution for approximately 15 s. LEICA DM2500 optical microscope was used to observe the microstructure.

2.4 Roughness Measurement

A portable roughness tester TR100 was used to measure the average surface roughness from five measurements on each sample at different positions. After machining, the samples were cleaned ultrasonically. 0.25 mm was the cut depth length and 8 mm was the racing length for the calculation of R_a, the roughness parameter (arithmetic average of absolute values).

2.5 Polarization Experiments

A round bottom cell was used for electrochemical investigations and all polarization tests were carried out in a potentiostat (Model 2263, Princeton Applied Research, USA). The electrochemical experiments were performed in 3.5% NaCl solution under fully aerated condition at ambient temperature of 26-28 °C. All the machined samples were cleaned with water, and then ultrasonically cleaned with acetone. The test was performed in a round bottom cell with graphite electrode as the counter electrode and saturated calomel electrode (SCE) as the reference electrode (E_{SCE} = ±241 mV). For each experiment, the working electrode was centrally located in the cell with three carbon electrodes as counter electrodes to ensure good current distribution. The reference electrode was exposed to solution through a luggin capillary filled with agar-agar gel. The polarization scan was conducted at ±250 mV with respect to open circuit potential (OCP) at a scan rate of 0.166 mV/s after stabilizing the potential at OCP for 1 h. The corrosion rate was estimated from the equation as per ASTM G102-89: The corrosion current density (i_{corr}) was obtained graphically using the polarization curve. The corrosion rates (mm/year) were calculated from the i_{corr} according to Tafel extrapolation method by extending the linear portions of the anodic and cathodic branches to a horizontal line drawn on E_{corr}. Linear parts of anodic and cathodic branches were used for the measurement of anodic and cathodic slopes. The Faraday's law was used to calculate the corrosion rate

$$\text{Corrosion rate} = \frac{i_{corr} M}{nF\rho}, \qquad \text{(Eq 1)}$$

where, i_{corr} is the corrosion current density in A/cm^2, W is the atomic weight of the element (55.85), ρ is the density of the element in gm/cm^3 (7.85 gm/cm^3), n is the number of electrons required to oxidize an atom of the element in the corrosion process, that is, the valence of the element (here it is taken as 2), and F is the Faraday's constant.

The corrosion rate was converted to mm/year by multiplying the right side of the Eq 1 with 3.154×10^8.

Table 1 Composition of steel used

C	Si	Mn	S	P	Ni	Cr	Mo	V
0.15	0.14	0.79	0.018	0.026	<0.010	0.013	0.004	0.003

2.6 Electrochemical Impedance Spectroscopy (EIS)

A sinusoidal potential perturbation of 10 mV, at open circuit potential, in frequency range of 100 kHz to 10 mHz was employed to obtain the impedance data. All experimental EIS data were modeled using ZSimpwin (version 3.10 Princeton Applied Research, USA) software and fitted using equivalent circuits.

3. Results and Discussion

3.1 Effect of Machining on Surface Microstructure

Figure 1(a) shows optical micrograph of the as-received annealed mild sample. The as-received sample shows equiaxed grains. Figure 1(b)-(d) shows the effect of cutting speed and rake angle on the surface optical microstructures of mild steel samples. It can be observed that with the increase in cutting speed, the surface grains experience shearing effect and grains try to align along the cutting direction (comparison of Fig. 1b and c). As the rake angle decreases, the shearing effect is extremely felt (comparison of Fig. 1b and d).

3.2 Polarization Behavior

3.2.1 Polarization Test. The polarization curves of the machined samples at different rake angles for low, medium, and high turning speeds are shown in Fig. 2(a)-(c), respectively, tested in freely aerated 3.5% NaCl solution.

The polarization results clearly depict that corrosion rate of machined samples (determined from i_{corr}) with positive tools rake angles are lower than corrosion rates of the samples machined at negative rake angles. As the speed increases for a constant rake angle, the corrosion rate also decreases as shown in Fig. 2(d). Interestingly, the electrochemical observations on the variation of corrosion rates with rake angle and cutting speed agree well with the results observed in case of immersion test (30 days) and salt fog test (21 days) discussed elsewhere in detail (Ref 16). Previous studies (Ref 16) reported by the authors on machined mild steel samples are presented in the form of comparative bar plots for immersion test (Fig. 3a) and salt fog exposure test (Fig. 3b). Both the tests have shown higher corrosion rates with decreasing rake angle, and lower corrosion rates with the increase in speed. The corresponding roughness values are also shown. It is observed that as the rake angle increases at a constant cutting speed, the roughness decreases. Interestingly, the corrosion rate has also decreased with increase in rake angle (Fig. 2 and 3). Similarly, at constant rake angle, the roughness decreases with increase in cutting speed and subsequently, the corrosion rates have also decreased. Hence, there is a strong correlation between the roughness and corrosion rate of mild steel. The overall conclusion that can be drawn from the Fig. 2 and 3 is that increase in roughness increases the corrosion rate. Another aspect is that the parameters, which would increase the roughness, would also increase the corrosion rate. It is interesting to note that with increase in cutting speed, the surface grains get sheared, and similarly with decrease in rake angle, the shearing effect is also felt (Fig. 1). This is also clear from the angle formed by two arrowheads showing the orientations of sheared grains and the cutting direction in case of Fig. 1(c) and (d). Since the shearing effect is more in case of −20° rake angle, the angle between the arrowheads is more acute than that in case of +20° rake angle. When the shearing is large, there would be the possibility of fewer grain boundaries to be exposed to corrosive solution. This would also result in less corrosion since grain boundaries are the heterogeneities, which are responsible for more corrosion attack. We have also shown this effect while discussing the effect of machining parameters on the oxidation behavior of mild steel in one of our

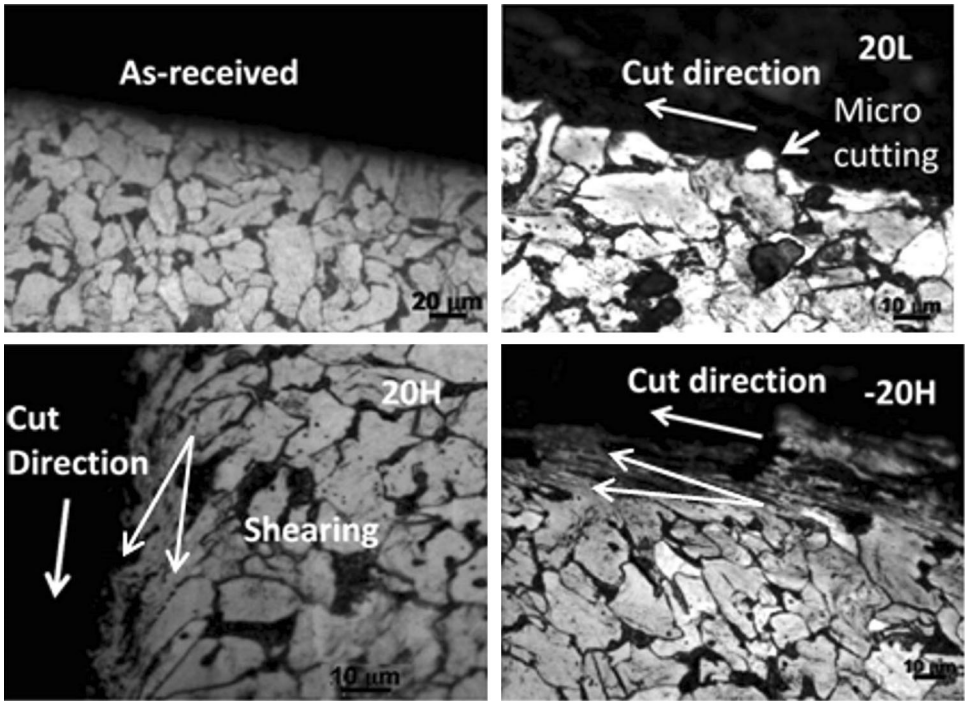

Fig. 1 Optical cross-sectional micrographs of the machined samples: (a) As-received annealed sample without machining, (b) 20 L, (c) 20 H, (d) −20 H

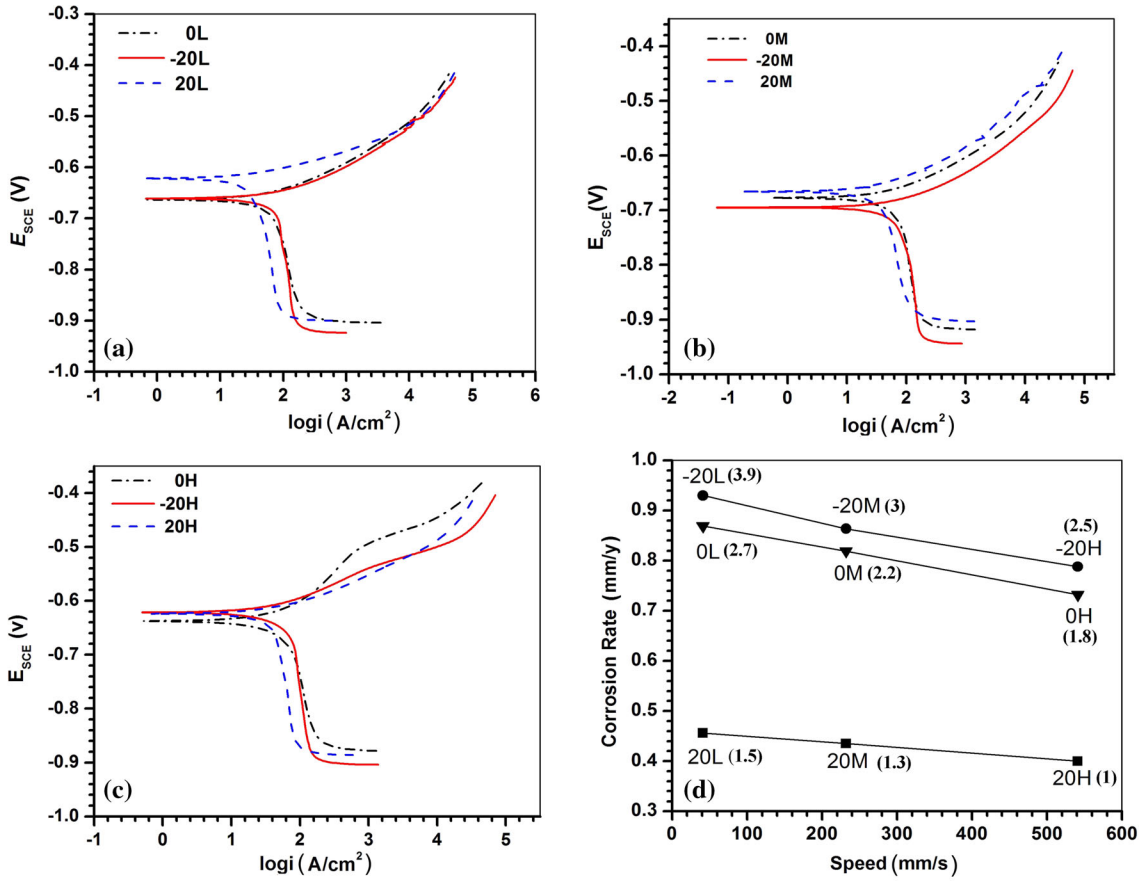

Fig. 2 Dynamic polarization plots of the machines samples in 3.5% NaCl solution (freely aerated) at different rake angles at cutting speeds of (a) 41 m/s, (b) 276 m/s, and (c) 541 m/s. (d) The corrosion rates of the machined samples. The bracketed values are the corresponding roughness value in μm for all the machined samples

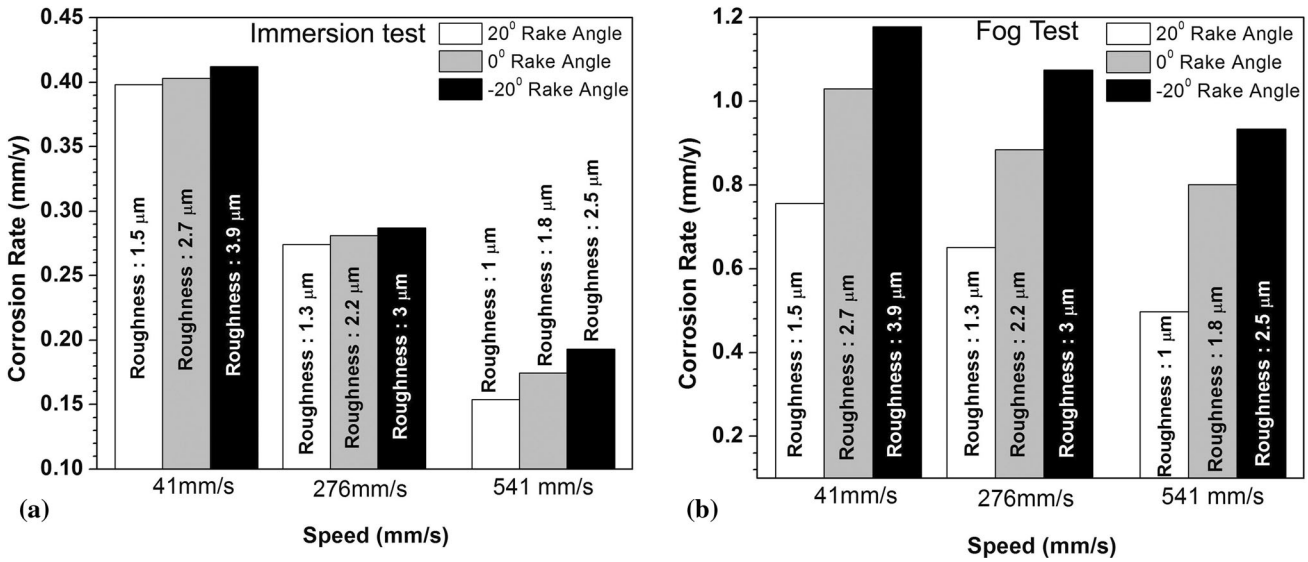

Fig. 3 The corrosion rate during (a) immersion and (b) salt fog test for the machined samples. The roughness values are also shown

previous communications (Ref 15). Figure 9(b) in Ref 15 shows schematically the effect of elongated grains on the oxidation behavior. The same figure shows that the elongation does lead to lesser grain openings to the surface (Ref 15). It has been observed from our earlier communication (Ref 16) that the pearlite gets spheroidized during machining due to adiabatic heating. It actually affects the corrosion behavior. Therefore, the morphology change in the pearlite is a critical factor for

Table 2 Corrosion parameters obtained from electrochemical polarization of machined samples in 3.5 wt.% NaCl

Samples	OCP (V_{SCE})	E_{corr} (V_{SCE})	β_a, V/decade	i_{corr}, μA/cm^2	Corrosion rate, mm/year
20 L	−0.632	−0.623	0.342	39.5	0.456
20 M	−0.628	−0.665	0.572	37.7	0.435
20 H	−0.622	−0.622	0.436	35.5	0.401
0 L	−0.659	−0.664	0.514	75.2	0.869
0 M	−0.648	−0.678	0.532	72.6	0.819
0 H	−0.636	−0.638	0.584	65.1	0.732
−20 L	−0.691	−0.668	0.456	80.5	0.930
−20 M	−0.674	−0.688	0.634	74.8	0.864
−20 H	−0.658	−0.620	0.550	68.2	0.788

deciding the electrochemical behavior of mild steel during machining, and it needs further analysis. More in-depth studies on the effect of microstructure evolution during machining and subsequent corrosion behavior are underway.

The parameters obtained from the polarization curves are shown in Table 2. OCP values of the machined samples determined before polarizing the test electrode follow a specific trend. Higher the rake angles, lower is the OCP, and the sample becomes nobler. On the contrary, higher the speed, lower is the OCP, and the sample becomes nobler. It suggests that the machining at negative rake angle (−20°) induces lot of straining as observed by the appearance of elongated surface grains (Fig. 2). This also increases the energy of the surface and activity. Hence, it would be active and its potential should go to cathodic side. This has actually been observed here (Table 2), that the sample, made at −20° rake angle, has got ∼−0.691 V_{SCE} OCP. On the contrary, the sample machined at 20° does not deform the surface grains of the sample to the extent what −20° does. Hence, it also shows nobility (Table 2; OCP ∼0.632 V_{SCE}). Moreover, the OCP values are also in good correlation with the roughness. With the increase in roughness, the OCP values have also gone more towards cathodic side. If the cutting speed is fixed, like 41 mm/s, the sample machined at +20° rake angle shows the noblest OCP because of its lowest roughness, and the sample machined at −20° shows most active OCP because of its largest roughness (Table 2; Fig. 3). The OCP of the sample machined at 0° rake angle lies in between at 41 mm/s cutting speed. Its roughness also lies in between (Table 2; Fig. 3). From Table 2 and Fig. 3, it is also clear that if the rake angle remains fixed, the sample with higher roughness (corresponding to lower cutting speed) has more active OCP. Roughness is associated with higher strain on the surface (Fig. 3 in Ref 16). That would definitely increase the activity of the surface and hence OCP. Other researchers have also noticed the similar behavior of OCP with roughness. Lee et al. (Ref 17) have shown that heavy mechanical deformation of SS304 steel leads to increase in surface roughness and drop in OCP. Liang et al. (Ref 18) have also shown that ball milling, which increases the roughness, also leads to drop in OCP of SS304 steel. Similarly, Souza et al. (Ref 19) have also shown the similar behavior of dropping of OCP with increase in roughness of galvanized steel during tribo-corrosion study.

In case of lower speed of cutting, the heat generated due to deformation and friction at the tool and sample junction has the time to dissipate. However, in case of higher cutting speed, the time required for heat dissipation is less and the heat can increase the temperature of the surface grains due to adiabatic nature and strain could be relieved a bit. There could be possibility of structural changes too. Previous study (Ref 16) has indeed shown spheroidization of the pearlite. Hence, the sample made at lower cutting speed would then have maximum activity as per potential is concerned since there is little chance of strain relieve. This has actually been observed here too. The sample with lower speed has got the OCP on the anodic side suggesting active nature (Table 2). The cathodic slopes for the machined samples indicate diffusion-controlled polarization and possible cathodic reaction in fully aerated solution could be ($O_2 + 2H_2O + 4e = 4OH^-$). The corresponding corrosion current potential (E_{corr}) of different mild steel samples determined from the polarizing curve is given in Table 2.

3.2.2 Electrochemical Impedance Spectroscopy Studies. Electrochemical impedance spectra of the machined samples with constant rake angle and different speed are depicted in Fig. 4(a)-(c), and those of the samples with constant speed and varying rake angle are shown in Fig. 4(d)-(f). The spectra have been presented as Nyquist plots (Fig. 3a and d), Bode magnitude (Fig. 4b and e), and Bode phase (Fig. 4c and f). The equivalent circuit R_s (C_{dl} R_c) used to fit the data is shown in Fig. 4(g) on the basis of least Chi square (χ^2) value. R_s refers to solution resistance of the test electrolyte (3.5% NaCl), C_{dl} is the capacitance of the electric double layer (EDL), and R_c is the charge transfer resistance between metal and electrolyte and also refers to polarization resistance.

The nature of the Nyquist plot shows similar behavior for all machined samples consisting of an incomplete semicircle that can be extrapolated to a semicircle and is associated with the corrosion process. The R_c has been determined from the diameter of the Nyquist plot. As shown in Table 3, the corresponding values of R_c obtained from fitting show distinct values for different cases of machined samples. R_c value is maximum in case the 20 H machined sample indicating higher charge transfer resistance between metal and electrolyte interface compared to that of the 20 M and 20 L sample (Fig. 4a). Similarly, the R_c value of the 20 M is higher compared to that of the 0 M and −20 M sample (Fig. 4b). The trend is similar. Higher the cutting speed, higher is the charge transfer resistance (Table 3). Lower the rake angle, lower is the charge transfer reactions. The relation between the R_c and machining parameters would possibly depend on the roughness again. It has been noticed that higher the roughness, greater is the drop of OCP values towards cathodic side. It suggests that active behavior of the sample with higher roughness would also allow the charge to transfer easily in the double layer leading to higher corrosion current (Tables 2 and 3).

The Nyquist plots are representatives of all nine samples. Therefore, the samples made at lower cutting speeds would definitely possess more dissolution since they have got lower charge transfer resistances (Fig. 4a). On other side, the samples

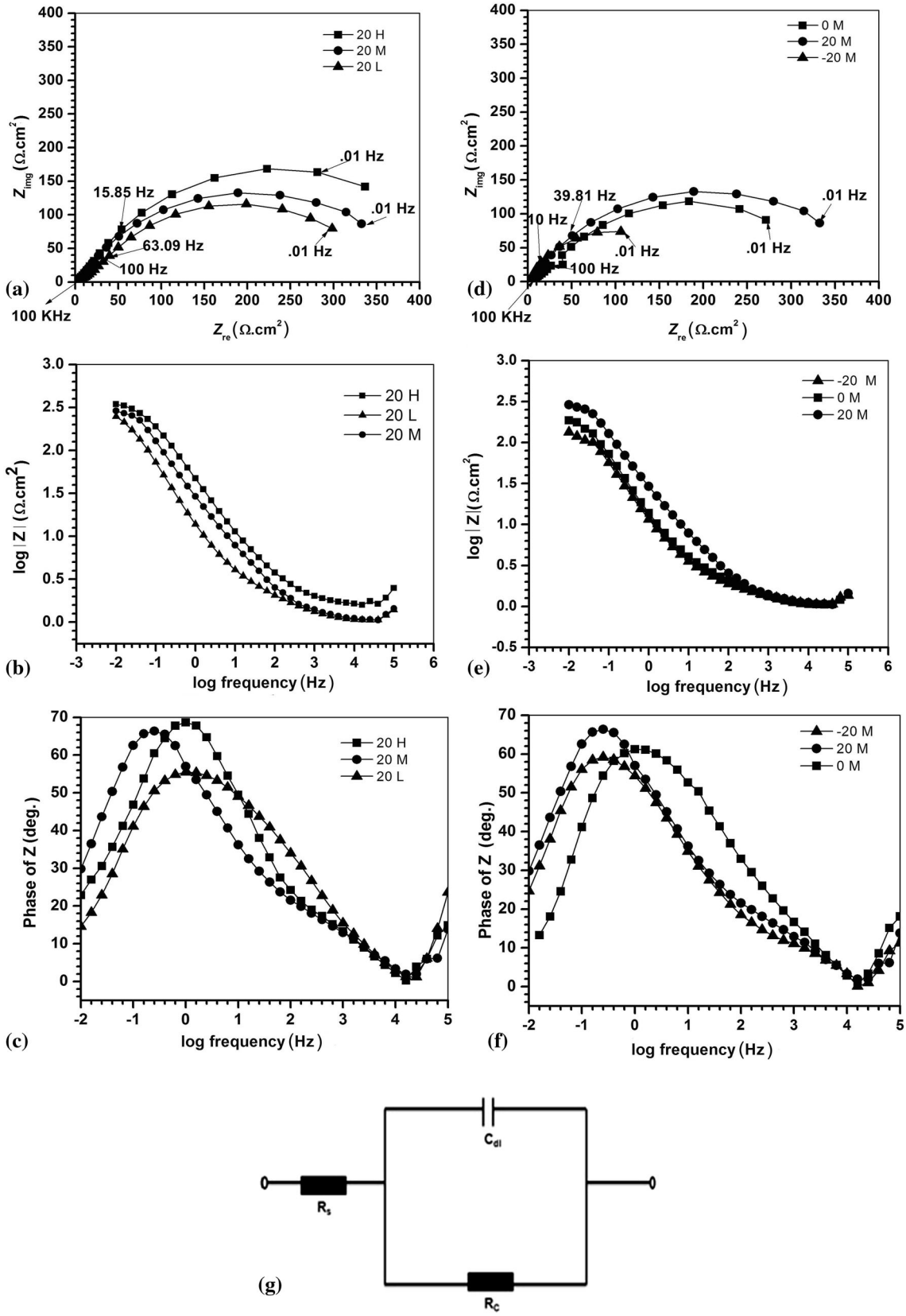

Fig. 4 (a) Nyquist, (b) Bode magnitude, and (c) Bode phase plots of the machined samples at 20° rake angle and speed L, M, and H. (d) Nyquist, (e) Bode magnitude, and (f) Bode phase plots of the machined samples at speed M, and varied rake angles 0°, 20°, and −20° and (g) model used to fit EIS data

Table 3 Data measured from EIS measurement at open circuit potential (OCP) in 3.5% NaCl solution simulated using the equivalent circuit

Sample	R_S, Ω cm^2	C (×10^{-3} F cm^2)	R_c, Ω cm^2	χ^2 (Chi squared)
20 H	4.934 (3.89)	1.391 (2.23)	447.3 (2.58)	2.703×10^{-1}
20 M	4.434 (2.89)	1.993 (3.23)	372.9 (2.96)	1.703×10^{-1}
20 L	4.505 (4.972)	1.398 (2.81)	347.5 (2.97)	1.078×10^{-1}
0 H	4.396 (3.79)	2.399 (6.13)	343.2 (2.75)	1.647×10^{-1}
0 M	4.509 (3.27)	1.836 (8.01)	338.3 (2.96)	2.938×10^{-1}
0 L	4.861 (2.192)	4.168 (5.85)	232.6 (8.49)	0.784×10^{-1}
−20 H	4.651 (1.02)	3.712 (4.88)	185 (6.07)	0.749×10^{-1}
−20 M	4.525 (4.859)	1.982 (3.69)	181.8 (7.31)	0.070×10^{-1}
−20 L	3.871 (5.45)	2.619 (2.34)	174.7 (5.24)	0.777×10^{-1}

made at lower rake angle would definitely show higher dissolution since they have lower charge transfer resistances (Fig. 4b). Interestingly, similar nature of dissolution rates was observed from i_{corr} and subsequent corrosion rates (Table 2; Fig. 2d).

The results obtained from the Nyquist plots are confirmed from Bode magnitude plots. The Bode magnitude plots (Fig. 4b and e) show higher polarization resistance for the 20H sample compared to that of the 20 L and 20 M, and higher for the 20 M as compared to the −20 M and 0 M sample. The Bode phase plots as shown in Fig. 4(c) and (f) indicate single maximum for all the three materials indicating the presence of a single time constant. A single time constant is indicative of the fact that all the machined mild steels samples corrode freely in presence of chloride ions. The Bode magnitude and Bode phase plots show one maximum value and one negative slope for each sample. The horizontal part in the Bode magnitude plots (Fig. 4c and d) indicates frequency independent region and corresponds to pure resistance. The linear slope of the Bode magnitude plot is the characteristic response of the capacitive behavior of the electrode double layer (Ref 20-22).

The Bode phase plot (Fig. 4c) shows that the maxima of the 20 H sample is closer to 90° indicating a better capacitive behavior of the double layer compared to that of the 20 M and 20 L machined samples. The shifting of the Bode phase curve of the 20 H sample towards higher frequency indicates a reduction in the value of C_{dl}. Figure 4(f) shows that the 20 M sample has maxima close to 90° compared to the −20 M and 0 M samples suggesting better capacitive behavior (Ref 20). There is an indication of single maxima in Bode phase plot. However, the same is indicated by the Nyquist plots. Further on modeling using equivalent circuits (R_s (C R_c)), it has been observed that the best fit is obtained using simple Randle's circuit, thus confirming the presence of single maxima. The capacitance values of the 20 H and 20 L samples are observed to be similar compared to the 20 M sample, which is higher (Fig. 4c). The capacitance values of the 20 M and −20 M samples are observed to be similar, whereas as for the 0 M sample it is less (Fig. 4f). The R_s, R_c, and C values for all machined samples are listed in Table 3.

With increasing rake angle, the R_c values increase. For constant rake angle and increasing speed, the R_c values increase showing less charge transfer between the metal and electrolyte interface leading to higher charge transfer resistance. The low roughness of the samples at high rake angles and high speed at constant rake angle can be one reason for high R_c values. The corrosion rates as observed in the machined samples also have exhibited good correlation with the machined surface conditions. The roughness values of different samples are mentioned in Fig. 3. In the earlier work, it has been shown that it is not only the roughness, but surface grain morphology also equally plays important role in the corrosion behavior of the samples. The surface grain morphology and roughness are also intimately associated with rake angle and cutting speed. It is interesting that the corrosion rates as observed from the i_{corr} values (Table 2; Fig. 2d), show similar trend as observed in case of immersion and salt fog tests (Fig. 3) though the values of corrosion rates are different. This is obvious since immersion and salt fog tests are long duration tests as well aggressive tests. Therefore, it can be concluded that the i_{corr} and polarization influencing factors like R_c, R_p, and C have got the similar relation to roughness as well as surface grain morphology.

4. Conclusions

Electrochemical polarization test was carried out on mild steel samples to study the effect of machining configuration, surface morphology, and surface roughness on electrochemical and corrosion behavior in 3.5% NaCl. The turning operations on mild steel at different rake angles and speeds have resulted in surfaces with varied surface finish and surface grain morphology. The findings can be summarized as follows:

1. Polarization tests show corrosion rates (i_{corr}) increasing with decreasing rake angle, and decreasing with the increase in speed.
2. Electron impedance spectroscopy measurements demonstrate a high charge transfer resistance, R_c for the samples at positive rake angle and high speed. There is direct relation of R_c with the corrosion rates as determined from Tafel polarization.

Further, the above results are in close agreement with the results obtained on immersion and fog test studies and suggest that machining on mild steel should be carried out at positive rake angle and at higher speed to get smoother surface and possibly for better corrosion performance.

Acknowledgment

The work has been supported by the Indian Space Research Organization, India (Project No: STC/MET/20120330).

References

1. C.Y. Nian, W.H. Yangand, and Y.S. Tarng, Optimization of Turning Operations with Multiple Performance Characteristics, *J. Mater. Process. Technol.*, 1999, **95**, p 90–96
2. K. Hussain, D.S. Wilkinson, and J.D. Embury, Effect of Surface Finish on High Temperature Fatigue of a Nickel Based Super Alloy, *Int. J. Fatigue*, 2009, **31**, p 743–750
3. R. Dubovska, J. Jambor, and J. Majerik, Qualitative Aspects of Machined Surfaces of High Strength Steels, *Procedia Engineering 24th DAAAM International Symposium on Intelligent Manufacturing and Automation 2013*, 2014, 69, p 646–654
4. S. Ghosh and V. Kain, Microstructural Changes in AISI, 304L Stainless Steel Due to Surface Machining: Effect on Its Susceptibility to Chloride Stress Corrosion Cracking, *J. Nucl. Mater.*, 2010, **403**, p 62–67
5. J. Cai, S. Shekhar, J. Wang, and M.R. Shankar, Nanotwinned Microstructures from Low Stacking Fault Energy Brass by High-Rate Severe Plastic Deformation, *Scr. Mater.*, 2009, **60**, p 599–602
6. S.G. Lee, J.H. Hwang, M.R. Shankar, S. Chandrasekar, and W.D. Compton, Large Strain Deformation Field in Machining, *Metall. Mater. Trans.*, 2006, **37A**, p 1633–1643
7. S. Swarninathan, M.R. Shankar, S. Lee, J. Hwang, A.H. King, R.F. Kezar, B.C. Rao, T.L. Brown, S. Chandrasekar, W.D. Compton, and K.P. Trumble, Large Strain Deformation and Ultra-Fine Grained Materials by Machining, *Mater. Sci. Eng. A*, 2005, **410**, p 358–363
8. S. Shekhar, S. Abholghasem, S. Basu, J. Cai, and M.R. Shankar, Effect of Severe Plastic Deformation in Machining Elucidated via Rate-Strain-Microstructure Mappings, *J. Manuf. Sci. Eng.*, 2012, **134**, p 031008–031019
9. M. Yamashita, H. Miyukl, Y. Matsuda, H. Nagano, and T. Misawa, The Long Term Growth of the Protective Rust Layer Formed on Weathering Steel by Atmospheric Corrosion During a Quarter of a Century, *Corros. Sci.*, 1994, **36**, p 283–299
10. T. Misawa, K. Asami, K. Hashimoto, and S. Shimodaira, The Mechanism of Atmospheric Rusting and the Protective Amorphous Rust on Low Alloy Steel, *Corros. Sci.*, 1974, **14**, p 279–289
11. J.M. Costa, M. Morcillo, and S. Feliu, Effect of Environmental Parameters on Atmospheric Corrosion of Metals, Encyclopedia of Environmental Control Technology, *Air Pollut. Control*, 1989, **2**, p 197–238
12. D. de la Fuente, I. Díaz, J. Simancas, B. Chico, and M. Morcillo, Long Term Atmospheric Corrosion of Mild Steel, *Corros. Sci.*, 2011, **53**, p 604–617
13. S.J. Oha, D.C. Cook, and H.E. Townsend, Atmospheric Corrosion of Different Steels in Marine, Rural and Industrial Environments, *Corros. Sci.*, 1999, **41**, p 1687–1702
14. J. Gravier, V. Vignal, and S.S. Bissey-Breton, Influence of Residual Stress, Surface Roughness and Crystallographic Texture Induced by Machining on the Ion Behaviour of Copper in Salt-Fog Atmosphere, *Corros. Sci.*, 2012, **61**, p 162–170
15. P. Mazumdar, S. Shekhar, and K. Mondal, Effect of Machining Parameters on Oxidation Behavior of Mild Steel, *J. Mater. Eng. Process.*, 2015, **24**, p 484–498
16. M. Prakash, S. Shekhar, A.P. Moon, and K. Mondal, Effect of Machining Configuration on the Corrosion of Mild Steel, *J. Mater. Process. Technol.*, 2015, **219**, p 70–83
17. H. Lee, D. Kim, J. Jung, Y. Pyoun, and K. Shin, Influence of Pinning on the Corrosion Properties of AISI, 304 Stainless Steel, *Corros. Sci.*, 2009, **51**, p 2826–2830
18. J. Liang, M.A. Wahab, and S.M. Guo, Corrosion Behavior of SS304 with Ball Milling and Electrolytic Plasma Treatment in NaCl Solution, in Mechanics of Time Dependent Materials and Processes in Conventional and Multifunctional Materials, *Conference Proceedings of the Society for Experimental Mechanics Series 99999*, T. Proulx, Ed., 2011, p 73–80
19. M.E.P. Souza, E. Ariza, M. Ballester, L.A. Rocha, and C. Freire, Comparative Behaviour in Terms of Wear and Corrosion Resistance of Galvanized and Zinc-Iron Coated Steels, *Revista Matéria*, 2007, **12**, p 618–623
20. B. Panda, R. Balasubramaniam, and G. Dwivedi, On the Corrosion Behaviour of Novel High Carbon Rail Steels in Simulated Cyclic Wet-Dry Salt Fog Conditions, *Corros. Sci.*, 2008, **50**, p 1684–1692
21. A. Moon, S. Sangal, and K. Mondal, Corrosion Behaviour of New Railway Axle Steels, *Trans. Indian Inst. Met.*, 2013, **66**, p 33–41
22. A. Moon, S. Sangal, S. Srivastav, N.S. Gajbhiye, and K. Mondal, Corrosion Behavior of IF Steel in Various Media and Its Comparison with Mild Steel, *J. Mater. Eng. Perform.*, 2015, **25**, p 85–97